Desalination and Water Treatment
www.deswater.com
doi: 10.5004/dwt.2019.24721

170 (2019) 211–224
December

Anti-crushing millimeter composite beads for removing 2,4-dichlorophenoxyacetic acid from aqueous solution

Sheng Feng[a,*], Xianglin Huang[a], Guiliang Zhu[a], Wei Zheng[a], Cong Shao[a], Ning Zhou[b]

[a]*School of Environmental and Safety Engineering, Changzhou University, Jiangsu 213164, China, Tel. +86-519-86330080; emails: shfeng@cczu.edu.cn (S. Feng), xianglhuang@163.com (X.L. Huang), zhuguiliang940606@qq.com (G.L. Zhu), ZW17862930738@163.com (W. Zheng), CongShaoCCZU@outlook.com (C. Shao)*
[b]*School of Petroleum Engineering, Changzhou University, Jiangsu 213164, China, email: zhouning@cczu.edu.cn*

Received 19 December 2018; Accepted 24 July 2019

ABSTRACT

The millimeter composite bead with enhanced crush resistance, UiO-66/chitosan@UiO-66 (UCU), can be fabricated by depositing UiO-66 nanoparticles on the surface of bead. In the experiment, the sample was characterized by X-ray powder diffraction, Fourier transform infra-red, Brunauer–Emmet–Teller, scanning electron microscopy, transmission electron microscope and zeta potential. The effects of time, concentration, pH, temperature and number of cycles on the adsorption of 2,4-dichlorophenoxyacetic acid by UCU were observed. The results revealed that in comparison with chitosan (CS), CS@UiO-66 and UiO-66/CS, UCU showed better adsorption capacity, and the Langmuir isotherm model appropriately described the adsorption (the q_{max} of UCU was 302.11 mg g^{-1}). After five cycles, the adsorption capacity of UCU still reached a high level (>85%). Different from no-load or internal-load UiO-66, the surface deposition can effectively enhance the crushing resistance of beads. Through the analysis on the adsorption mechanism, it was found that the strong electrostatic interaction dominated the adsorption, which was accompanied by weak π–π stacking.

Keywords: Adsorption; UiO-66; Chitosan; 2,4-D

1. Introduction

In the past 20 years, pharmaceutical and personal care products (PPCPs) have become important constituents of emerging concerns [1,2]. With the improvement of human living standards, the application of PPCPs has increased [3–6]. However, the untreated emissions have caused more and more serious environmental hazards [7,8]. PPCPs continue to have adverse effects on humans and animals by transferring to foods such as vegetables and fish [9,10]—disrupting endocrine and producing other side effects [11]. 2,4-dichlorophenoxyacetic acid (2,4-D), one of the representatives of PPCPs, is a fairly toxic contaminant, which has been proven to be an endocrine disruptor to irritate human skin and eyes with long-term exposure [12–14]. Due to the widespread application of 2,4-D, many surveys concerning concentration in current years have reported the presence of 2,4-D in surface water and groundwater [15,16], increasing the risk of ecological damage [17,18]. There are many methods to remove 2,4-D from liquid phase, such as photocatalytic degradation [19,20], biodegradation [21,22], ozone oxidation [23] and adsorption [24,25]. However, most of the methods are costly and ineffective. In contrast, adsorption is one of the most competitive methods for 2,4-D due to its economy, simplicity and convenience.

Metal-organic frameworks (MOFs) have cage structures formed by metal nodes in connection with organic ligands. They have been extensively researched for gas adsorption and storage [26,27], as well as for removing many water contaminants. UiO-66 is a sort of MOF with Zr^{4+} as the metal node and phthalate (BDC) as the connector. Due to its high water-stability, UiO-66 is often researched to remove pollutants in water [28,29]. However, the recovery of UiO-66

* Corresponding author.

is inconvenient. Moreover, it usually requires a large amount of post-treatment to separate the adsorbent from aqueous solution, which is a defect in practical applications. This problem can be easily solved by loading UiO-66 on millimeter chitosan (CS) beads [30]. CS is a product, which is synthesized by the deacetylation of chitin. It can be widely found in the world [31,32], such as the shell of crustaceans. As the only natural cationic biopolymer in nature, it has been applied in many fields, such as medicine, flame retardant materials and food science [33]. Due to the non-toxic, biocompatible, biodegradable, cost-effective characteristics, CS has long been regarded as a potential and harmless adsorbent. It has excellent adsorption capacity for heavy metal ions and dyes [34–39], and has also been attempted to adsorb 2,4-D [40]. Although the internal load of UiO-66 can achieve the purpose of improving the adsorption capacity and facilitating recovery, the composite bead is as fragile as the pure CS bead.

In this work, a large amount of UiO-66 nanoparticles were deposited on the surface of the CS beads and UiO-66/CS to fabricate anti-crushing millimeter beads (CS@UiO-66 and UiO-66/chitosan@UiO-66 (UCU)). These composite beads were characterized by several precision instruments. The adsorption properties of the composite beads were evaluated by the adsorption experiments and analysis. Moreover, the crush resistance of a variety of beads was researched by vigorously oscillating them in water.

2. Experimental setup

2.1. Materials

2,4-D (97%), terephthalic acid (H_2BDC, 99%), sodium tripolyphosphate ($Na_5P_3O_{10}$, 98%), CS (degree of deacetylation ≥ 95%), diuron (99%), bentazon (99%), 2-methyl-4-chlorophenoxyacetic acid (MCPA, >98%) and glutaraldehyde (50% in H_2O) were obtained from Aladdin Industrial Corporation (809 Chuhua Branch Road, Chemical Industry Park, Yulin Town, Fengxian District, Shanghai, China). N,N-Dimethylformamide (DMF, ≥99.5%) and methanol (≥99.5%) were purchased from Chinasun Specialty Products Co. Ltd., (Baimao Industry Economy Development Zone, Changshu City, China). Zirconium chloride anhydrous ($ZrCl_4$, 98%) and hydrochloric acid (HCl, 36% ~ 38%) were provided by Sinopharm Chemical Reagent Co. Ltd., (52 Ning Bo Road, Shanghai, China). All of these drugs were applied without further purification.

2.2. Preparation of adsorbents

2.2.1. Preparation of UiO-66

First, UiO-66 was synthesized, according to the solvothermal method reported by Hasan et al. [41] (with slight modifications). $ZrCl_4$ (4 mmol) and H_2BDC (4 mmol) were added to DMF (25 ml). They were stirred until they were dissolved and mixed. Subsequently, they were added to a Teflon-lined autoclave (50 ml). After reacting at 120°C for 24 h, the resultant was washed for three times with DMF and methanol. Then, it was dried in a vacuum oven at 60°C for 12 h.

2.2.2. Preparation of beads

The detailed preparation process of CS beads was as follows: CS (0.8 g) was added to 40 ml of 1% by volume HCl solution, stirring for 6 h to form a uniform sol. The sol was slowly added drop by drop to a $Na_5P_3O_{10}$ solution (40 ml, $Na_5P_3O_{10}$ mass fraction of 1%) by applying a burette to form 1–2 mm precipitated beads immediately. Subsequently, the beads in the solution were kept incubated at 30°C for 10 h. After filtered and rinsed for three times with water, the beads were transferred to 0.02 mol L^{-1} glutaraldehyde solution to incubate at 40°C for 12 h. Then, it was washed again until the pH of the beads was neutral. Ultimately, it was lyophilized at –50°C for 10 h.

The preparation process of CS@UiO-66 beads was as follows: 1% of $Na_5P_3O_{10}$ solution (40 ml) was prepared, and then UiO-66 (0.4 g) was added to the solution and sonicated until it was completely dispersed to replace the $Na_5P_3O_{10}$ solution in the above operation. Subsequent operations were identical to the preparation of CS beads.

The preparations of UiO-66/CS beads and UCU beads only required the addition of UiO-66 nanoparticles (0.8 g) to the homogeneous sol according to the above description. Then, it was continued to stir until it was well-mixed. The subsequent operations were carried out according to the preparation methods of CS beads and CS@UiO-66 beads, respectively. The synthesis of UCU is shown in Fig. 1.

2.3. Characterization and measurement

The structures of samples were analyzed and confirmed by the patterns obtained from an X-ray powder diffractometer (XRD, Rigaku D/MAX2500PC, 3-9-12, Matsubara-cho, Akishima-shi, Tokyo, Japan). Simultaneously, the spectra of samples were taken through applying a Fourier transform infra-red spectrophotometer (FTIR, TENSOR 27) and the presence of major functional groups was analyzed and confirmed. The Brunauer–Emmet–Teller (BET) surface area and the Barrett–Joyner–Halenda (BJH) pore size of the adsorbents were described by the nitrogen adsorption–desorption curve measured through a gas adsorption instrument (Autosorb-iQ2/IQ, manufactured by Anton Paar, Anton-Paar-Straße 20, Graz, Styria 8054, Austria). The samples were degassed at 120°C for 2 h before analysis. The topography images of samples were taken by scanning electron microscope (SEM, Carl Zeiss Optics (China) Co. Ltd., 60 Meiyue Road, Shanghai Free Trade Zone, Shanghai, China), and the image of the sliced UCU was taken by transmission electron microscope (TEM, HT-7700). The powder samples of UCU were dispersed into eight pretreated ultrapure waters of different pH values (pH = 2.53, 3.36, 4.39, 5.24, 6.14, 6.83, 8.06 and 9.34). Subsequently, zeta potential (ZP) was measured with a ZETASIZER Nano-ZSP (Malvern, UK).

The adsorption procedure was as follows: a stock solution (200 ppm) was prepared by dissolving 2,4-D powder (200 mg) in deionized water (1,000 mL). Subsequently, it was diluted with deionized water to prepare the needed concentration (10–150 ppm) of solution. The pH adjustment was accomplished by dropwise addition of the formulated HCl solution (1 and 0.1 M) and NaOH solution (1 and 0.1 M) in the pH experiment. In addition to pH experiments, the pH values of all prepared solutions were adjusted to 3.5. 5 mg of adsorbents were added to each 50 mL of solution. The mixture was shaken at constant speed (150 rpm) for a predetermined time (0.25–24 h) in the water bath shaker. Except for thermodynamic experiment, the other adsorption experiments were

performed at 30°C. After adsorption, the solution was collected by applying a syringe and passed through a 0.44 μm filter. The remaining concentration of 2,4-D was calculated by measuring the absorbance value at 283 nm using a UV spectrophotometer. The amount of 2,4-D adsorbed under different conditions was calculated according to the following equation:

$$q_t = \left(\frac{C_0 - C_t}{m}\right) \times V \quad (1)$$

where C_0 (ppm) is the initial concentration of the solution and C_t (ppm) is the concentration of the solution at time; t, m (g) is the mass of the adsorbent, V (L) is the volume of the solution, and q_t (mg g^{-1}) is the amount of contaminant adsorbed by the sample at time t.

3. Results and discussion

3.1. Characterization of samples

The appearance of the four samples is shown in Fig. 2. The four sorts of beads have a similar particle size between 1 and 2 mm.

Fig. 3a illustrates that the other samples shown have good crystallinity except CS and CS@UiO-66, indicating that $Na_5P_3O_{10}$ has little effect on the crystal structure of UiO-66 [42]. Moreover, at the several main diffraction peaks of UiO-66 (2θ = 7.32°, 8.46°, 25.72° and 30.74°), it is observed that UiO-66/CS and UCU displays similarity, confirming

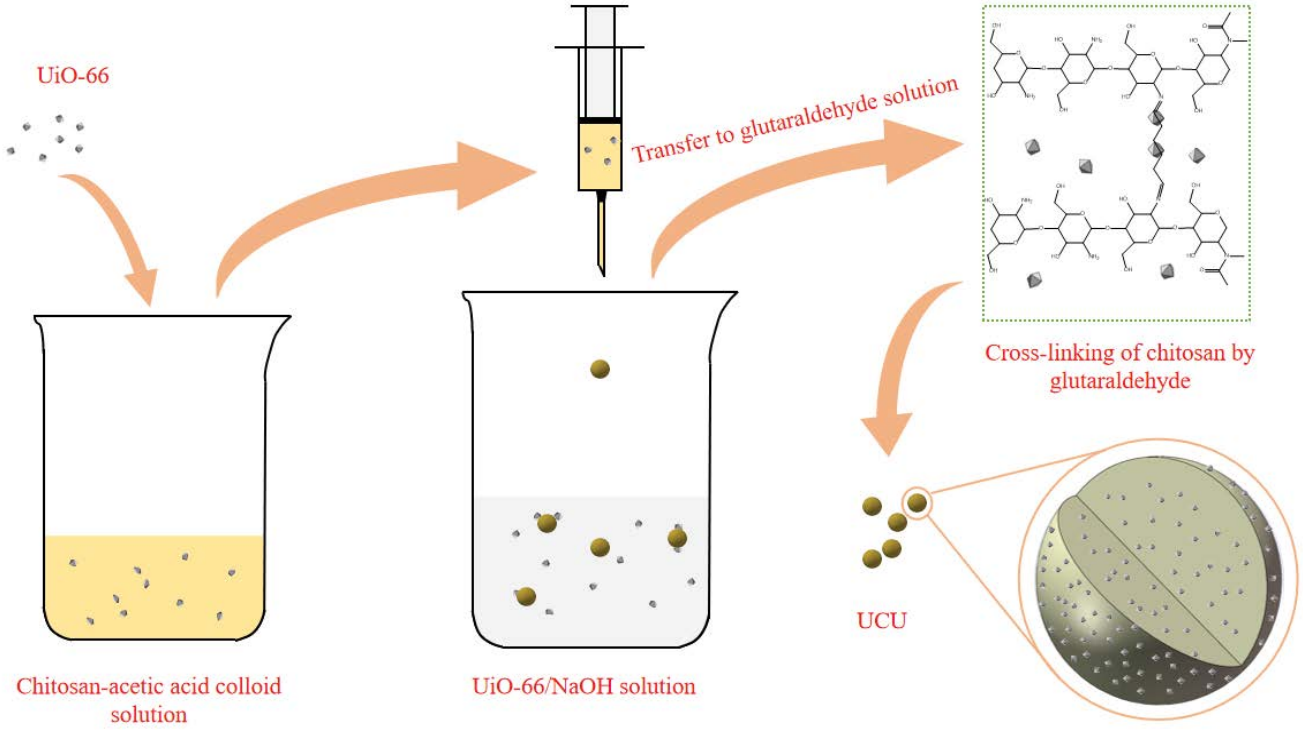

Fig. 1. Schematic diagram for the synthesis of UCU.

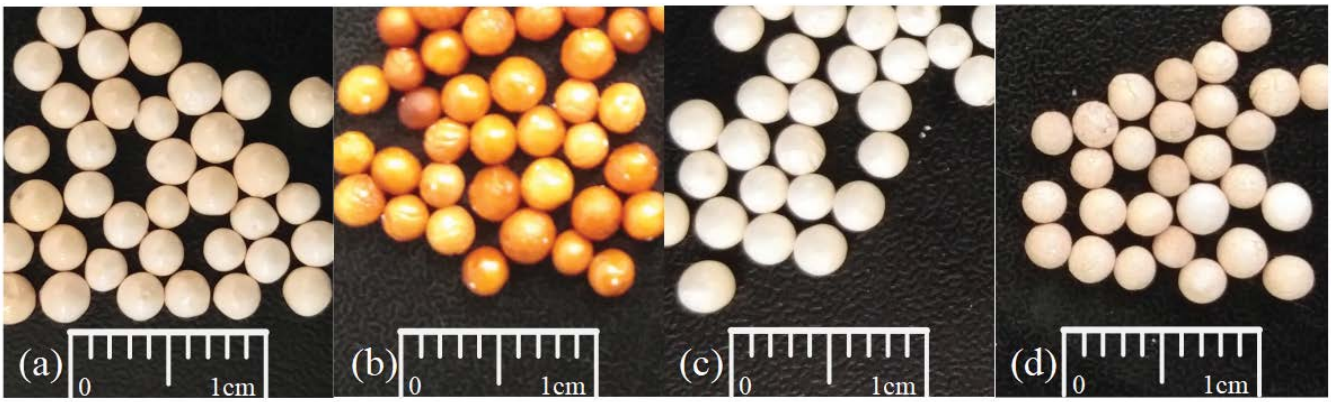

Fig. 2. Appearance of the four samples: (a) CS beads, (b) CS@UiO-66 beads, (c) UiO-66/CS beads and (d) UCU beads.

that UiO-66 are successfully added and maintain good crystallinity in both the samples. The intensity of the sample diffraction peak corresponds to the content of UiO-66. In comparison with UiO-66/CS, UCU obviously contains more UiO-66. Namely, UiO-66 is successfully loaded on its surface in addition to being mixed inside. For CS@UiO-66, the characteristic diffraction peak of UiO-66 is not observed because the content of UiO-66 in the sample is too small after grinding. However, in the FTIR spectrum, the presence of UIO-66 is found in the CS@UiO-66 sample. Fig. 3b indicates that UiO-66 has a medium intensity peak, which represents the Zr–μ_3–O stretching at 665 cm^{-1}. The similar peak is found in the spectra of CS@UiO-66, UiO-66/CS, and UCU, demonstrating that UiO-66 is successfully composited into these three samples. Except that, it is observed that the peaks of these three samples at 747 cm^{-1} (OH bending and CH bending (in-phase), 1,399 cm^{-1} (OCO symmetric stretching) and 1,507 cm^{-1} (CC ring) are associated with the original UiO-66, which also proves the presence of UiO-66 [43,44].

The N_2 adsorption and desorption isotherms of Fig. 4 clearly indicate the surface area relationship of the four sorts of beads (UCU > UiO-66/CS > CS@UiO-66 > CS). The specific surface area of the beads is positively correlated with the content of UiO-66., which means that the incorporation of UiO-66 can significantly increase the surface area of the adsorbents. The BET surface area and BJH pore size data are listed in Table 1. The BET surface area of UCU is almost 20 times more than that of the original CS. By the research on the BJH pore size, it is found that UCU has the smallest BJH average pore size among the four beads. The reason is that the incorporation of UiO-66 allows the sample to acquire more micropores, reducing the average pore size.

Fig. 5 visually reveals the surface and cross-sectional topography of the four sorts of beads. The pure CS bead has the smoothest surface in comparison with the other three beads. The surface of UiO-66/CS presents a small amount of uneven protrusions and holes. The protrusion is the indication of UiO-66, and the holes are caused by the incorporation of UiO-66, which affects the cross-linking of CS. On the surface of CS@UiO-66 beads, a large amount of UiO-66 is fixed by the cross-linking of ordered CS molecules to form a number of regularly arranged bumps. The UCU beads should have a similar surface to CS@UiO-66. However, the internal loading of UiO-66 disturbs the ordered arrangement of CS molecules, causing the surface of UiO-66 to become confusing. It can be ascertained that this disturbance does not affect the stability of the surface load as well as the anti-crushing ability of the outer shell. Fig. 5e shows that the distribution of UiO-66 inside the beads is equally uniform. It can also be seen in the cross-section of the beads that UiO-66 particles are evenly distributed inside the UiO-66/CS and UCU beads. In addition, according to the TEM image of Fig. 5j, it can be

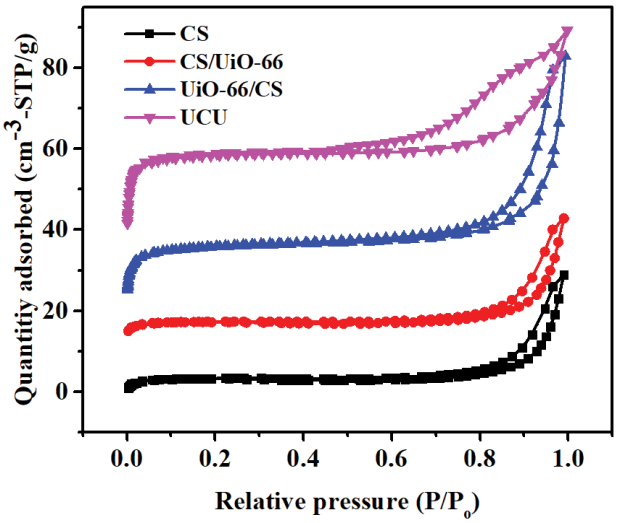

Fig. 4. N_2 adsorption and desorption isotherms of beads.

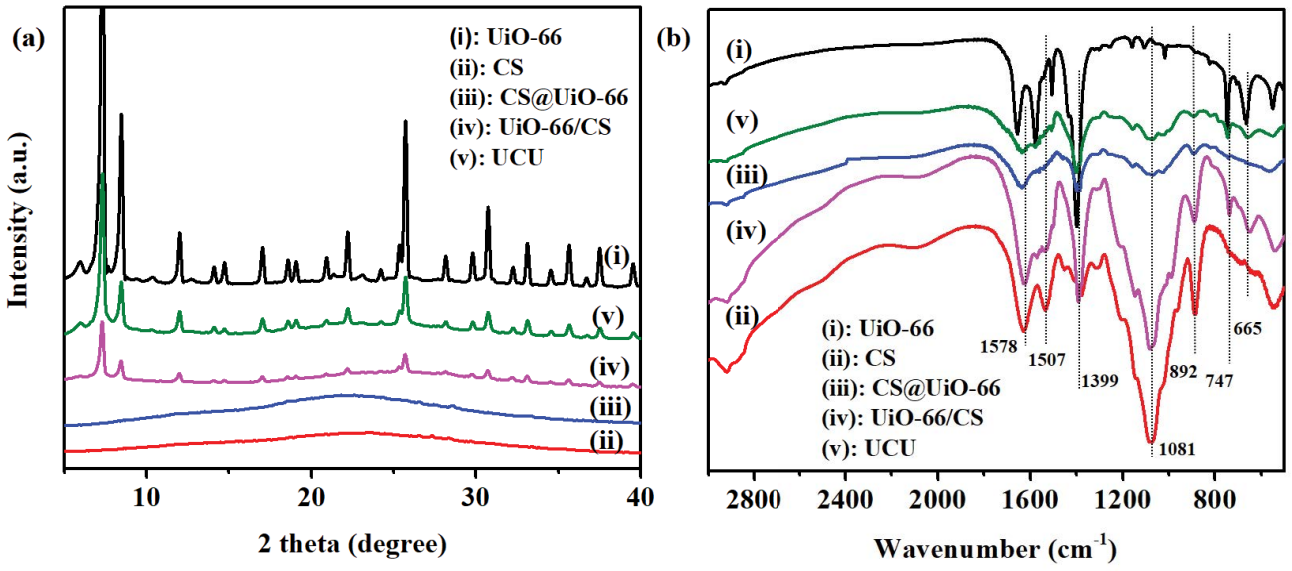

Fig. 3. (a) XRD patterns of UiO-66 and beads and (b) FTIR spectra of UiO-66 and beads.

Table 1
Surface area and BJH pore size of UiO-66 and beads

Adsorbent	BET surface area $m^2 g^{-1}$	Langmuir surface area $m^2 g^{-1}$	BJH adsorption average pore diameter (4 V/A) nm
UiO-66	888.37	1,313.19	5.63
CS	8.89	13.24	33.58
CS@UiO-66	28.59	42.32	33.14
UiO-66/CS	108.65	160.46	32.22
UCU	175.55	258.28	25.13

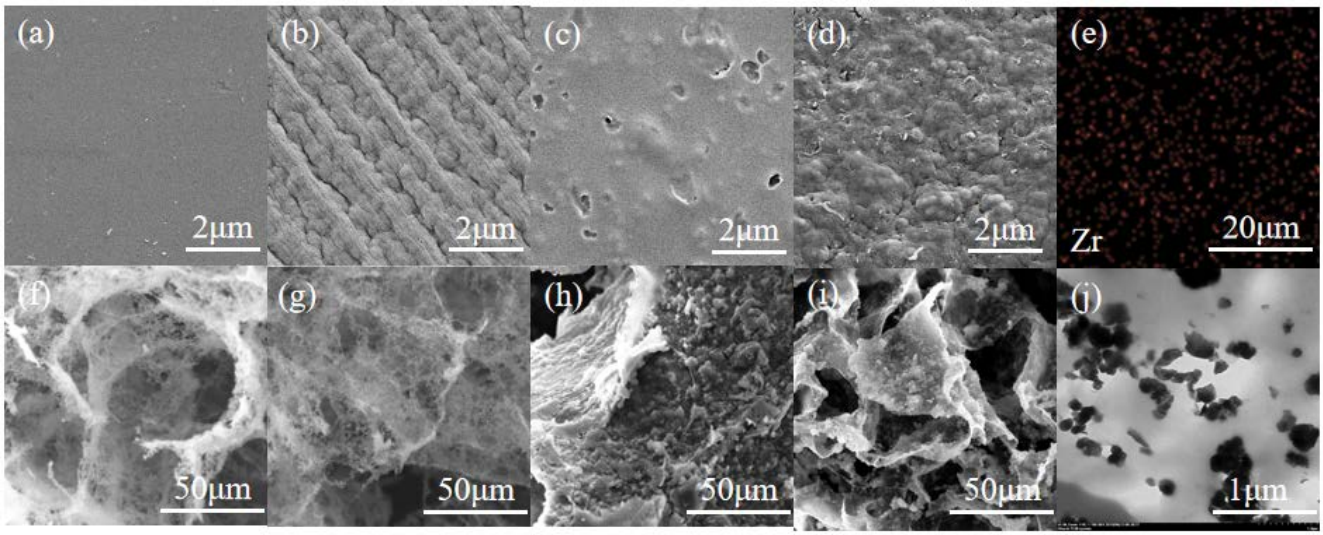

Fig. 5. Surface SEM images: (a) CS bead, (b) CS@UiO-66 bead, (c) UiO-66/CS bead, (d) UCU bead, (e) Mapping of Zr in UCU beads. Cross-section SEM images: (f) CS bead, (g) CS@UiO-66 bead, (h) UiO-66/CS bead, (i) UCU bead and (j) TEM image of UCU.

clearly seen that UiO-66 is encapsulated by CS and exhibits an excellent composite state.

3.2. Adsorption process

3.2.1. Concentration of 2,4-dichlorophenoxyacetic acid and adsorption isotherms

Fig. 6a indicates that the effect of 2,4-D concentration on the adsorption capacity of the different beads under same conditions. It can be concluded that the adsorption capacity at the same conditions follows a size relationship as UCU > UiO-66/CS > CS@UiO-66 > CS, which is consistent with the content of UiO-66. When the concentration reaches 150 ppm, the q_e values of these four adsorbents reach maximum. At this moment, the adsorption capacity of UCU (165.73 mg g^{-1}) is 2.03, 1.76 and 1.26 times that of CS (81.51 mg g^{-1}), CS@UiO-66 (94.02 mg g^{-1}) and UiO-66/CS (131.49 mg g^{-1}).

The adsorption isotherms were analyzed, applying the Langmuir and Freundlich models to evaluate adsorption. The Langmuir model describes a uniform adsorption state, while the Freundlich model expresses the heterogeneous adsorption. The Langmuir isotherm equation is expressed in Eq. (2) as follows:

$$\frac{C_e}{q_e} = \frac{1}{q_{\max} K_L} + \frac{C_e}{q_{\max}} \tag{2}$$

where C_e (ppm) is the concentration of 2,4-D when the adsorption process reaches equilibrium; q_e (mg g^{-1}) stands for the amount of 2,4-D removed by the adsorbent; $q_{\max}$ (mg g^{-1}) represents the theoretical maximum adsorption capacity that the adsorbent can achieve; K_L (L g^{-1}) refers to a Langmuir equilibrium constant related to adsorption capacity. The $q_{\max}$ was calculated from the slope of each line that fits the linear relationship between C_e/q_e and q_e in the Langmuir plot (Fig. 6b), and K_L was calculated from the intercept. The results are given in Table 2. UCU owns the highest K_L value, which reflects the best adsorption capacity.

R_L is a dimensionless parameter, which is applied to evaluate whether adsorption is favorable in the Langmuir model. The evaluation criteria are as follows: (1) irreversible (R_L = 0), (2) favorable (0 < R_L < 1), (3) linear (R_L = 1), (4) unfavorable (R_L > 1), adsorption can be simply classified according to these four criteria. The value of R_L can be calculated by the following equation:

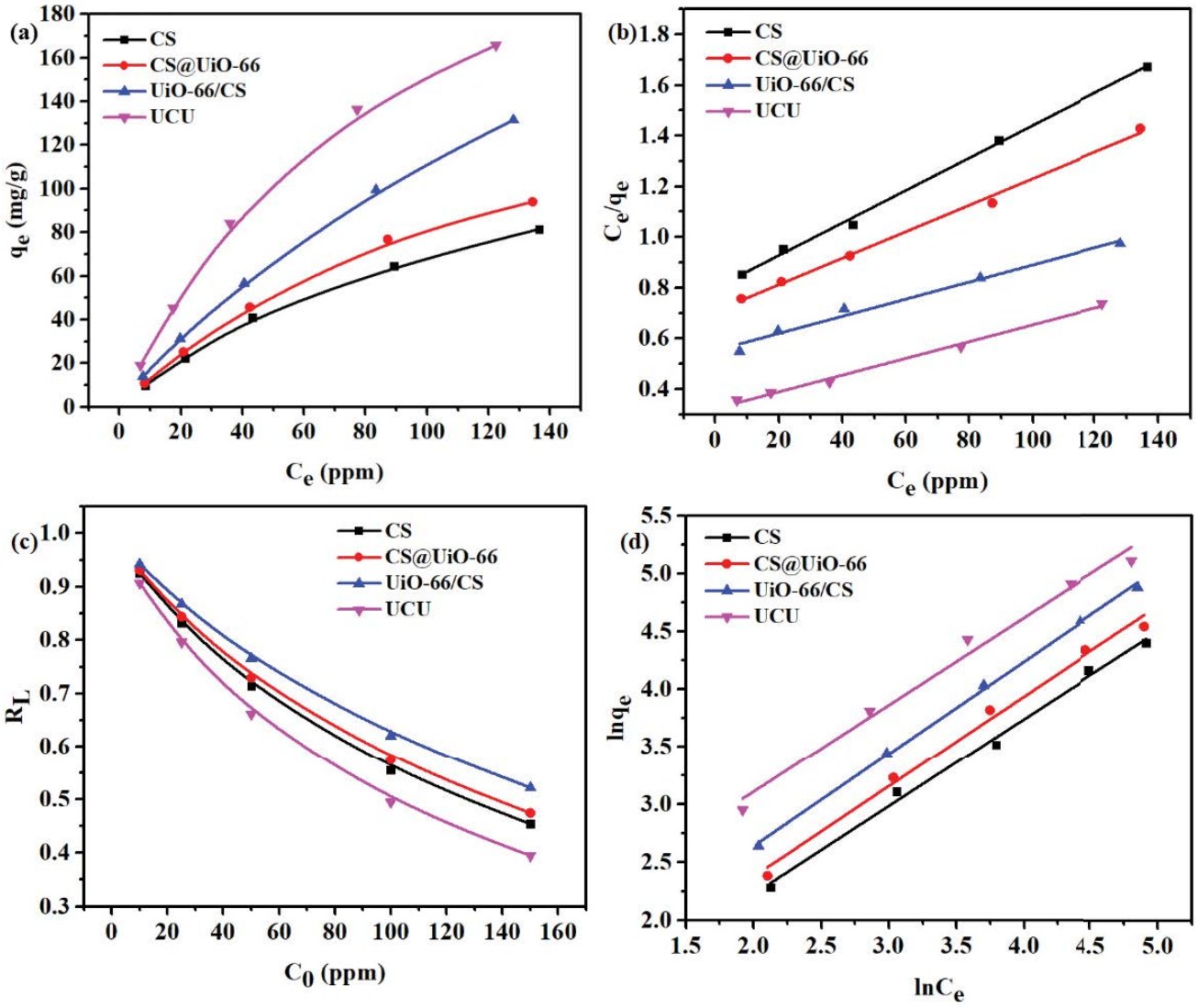

Fig. 6. (a) Adsorption isotherms, (b) Langmuir plot of the isotherm, (c) R_L of four beads and (d) Freundlich plot of the isotherm.

$$R_L = \frac{1}{1 + k_L C_0} \tag{3}$$

where C_0 (ppm) represents the initial concentration of 2,4-D. As shown in Fig. 6(c), all calculated R_L values are between 0 and 1, indicating that all adsorbents belong to the class which favors the adsorption of 2,4-D.

The Freundlich equation is expressed in Eq. (4) as follows:

$$\ln q_e = \ln k_F + \frac{1}{n} \ln C_e \tag{4}$$

where k_F (L g^{-1}) refers to the Freundlich constant related to the adsorption capacity, and $1/n$ stands for the parameter related to the adsorption strength. $1/n$ is the slope of each line obtained by fitting the linear relationship between $\ln C_e$ and $\ln q_e$ in the Freundlich plot (Fig. 6d), and k_F is calculated based on the intercept. The calculation results are also listed in Table 2. A high k_F value indicates an effective and positive adsorption. The details are illustrated in Fig. 6.

As is shown in Table 2, the R^2 values are data describing the correlation of the model with adsorption isotherms. The isotherms of CS, CS@UiO-66 and UCU are more compatible with the Langmuir model ($R^2 > 0.99$), indicating that their adsorption process is uniform, and electrostatic interaction may dominate the adsorption. Due to its high correlation coefficient ($R^2 = 0.9981$), the Freundlich model can describe the isotherms of UiO-66/CS better. In this way, we can see that the process may be heterogeneous.

In comparison with some previous studies (Table 3), the maximum adsorption capacity of UCU is superior to many micron or nano materials, which is almost equivalent to the q_{max} value of Fe/OMC.

Table 2
Isotherm parameters for adsorption of 2,4-D by four adsorbents

Adsorbent	Langmuir			Freundlich		
	K_L L g^{-1}	q_{max} mg g^{-1}	R^2	k_F L g^{-1}	$1/n$	R^2
CS	8.03	155.76	0.9966	2.03	0.76	0.9928
CS@UiO-66	7.39	191.20	0.9943	2.25	0.78	0.9891
UiO-66/CS	6.11	295.86	0.9786	2.81	0.80	0.9981
UCU	10.23	302.11	0.9918	4.93	0.76	0.9810

Table 3
Comparison of q_{max} values obtained from Langmuir isotherm model for 2,4-D adsorption on various adsorbents

Adsorbent	Particle size	q_{max} mg g^{-1}	References
UCU	Millimeter	302.1	This work
Carbon material synthesized by hexachlorobenzene combustion (C-C_6Cl_6)	Micron	89.5	[45]
Neem oil-phenolic resin treated jute (NJ)	Micron	38.5	[46]
Langsat empty fruit bunch activated carbon (LEFBAC)	Micron	261.2	[47]
Graphene oxide coated by porous iron oxide ribbons (GO-Fe_3O_4)	Nano	67.267	[48]
Magnetic halloysite nanotubes molecularly imprinted polymer (MHNTs@MIP)	Nano	39.4	[49]
Red mud@carbon composite (red mud@C)	Nano	111.1	[50]

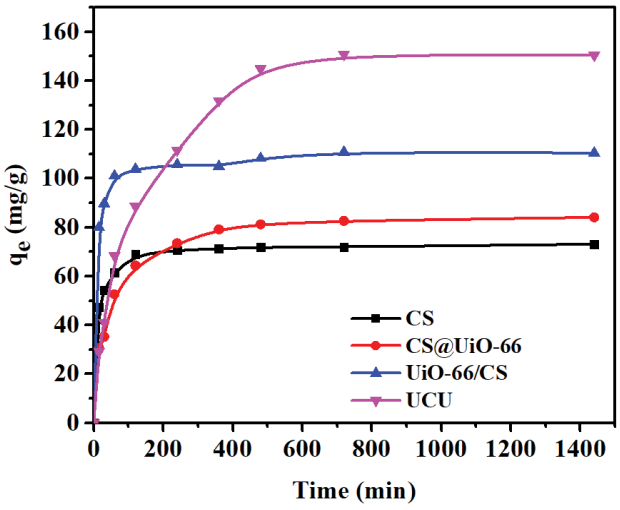

Fig. 7. Change in the amount of 2,4-D adsorbed by four adsorbents over time within 24 h.

3.2.2. Contact time and kinetics of adsorption

Fig. 7 displays the relationship between the amount of 2,4-D adsorbed by the four adsorbents and time. Both CS and UiO-66/CS reach the adsorption maximum within 120 min and remain near the maximum afterwards (69.72 and 103.90 mg g^{-1}). Meanwhile, the adsorption capacities of CS@UiO-66 and UCU are 64.39 and 88.61 mg g^{-1}. Comparing them with CS and UiO-66/CS, respectively, they need to spend more contact time about 80 min to reach the maximum of the comparison object. Moreover, the numbers will continue to increase and reach the maximum value with extra 200 min (110.85 and 150.87 mg g^{-1}). The adsorption equilibrium of CS and UiO-66/CS beads takes only a short time. For CS@UiO-66 and UCU beads, the surface loading of UiO-66 blocks part of the pores on the surface of the beads, making the 2,4-D molecules slower into the interior of the beads and reducing the adsorption rate of the beads.

To better understand the adsorption, the pseudo-first-order and pseudo-second-order kinetic models were applied to evaluate the kinetic mechanism of the adsorption process. The pseudo-first-order equation can be expressed by Eq. (5):

$$\ln(q_e - q_t) = \ln q_e - k_1 t \tag{5}$$

where q_e (mg g^{-1}) refers to the amount of 2,4-D, which is removed when the adsorption reaches equilibrium; q_t (mg g^{-1}) refers to the quantity of 2,4-D, which is adsorbed over the adsorbents at time t (min); k_1 (min^{-1}) represents the pseudo-first-order adsorption rate constant, which is determined by the linear relationship between $\ln(q_e - q_t)$ and t fitted in Fig. 8a. The calculation results and related data's are listed in Table 4.

The equation of pseudo-second-order is expressed in Eq. (6) as follows:

$$\frac{t}{q_t} = \frac{1}{k_2 q_e^2} + \frac{t}{q_e} \tag{6}$$

where k_2 (g mg^{-1} min^{-1}) represents a pseudo-second-order adsorption rate constant, which is determined by the intercept of the straight line obtained by fitting the relationship between t/q_t and t in Fig. 8b. The calculation results and related data's are also listed in Table 4.

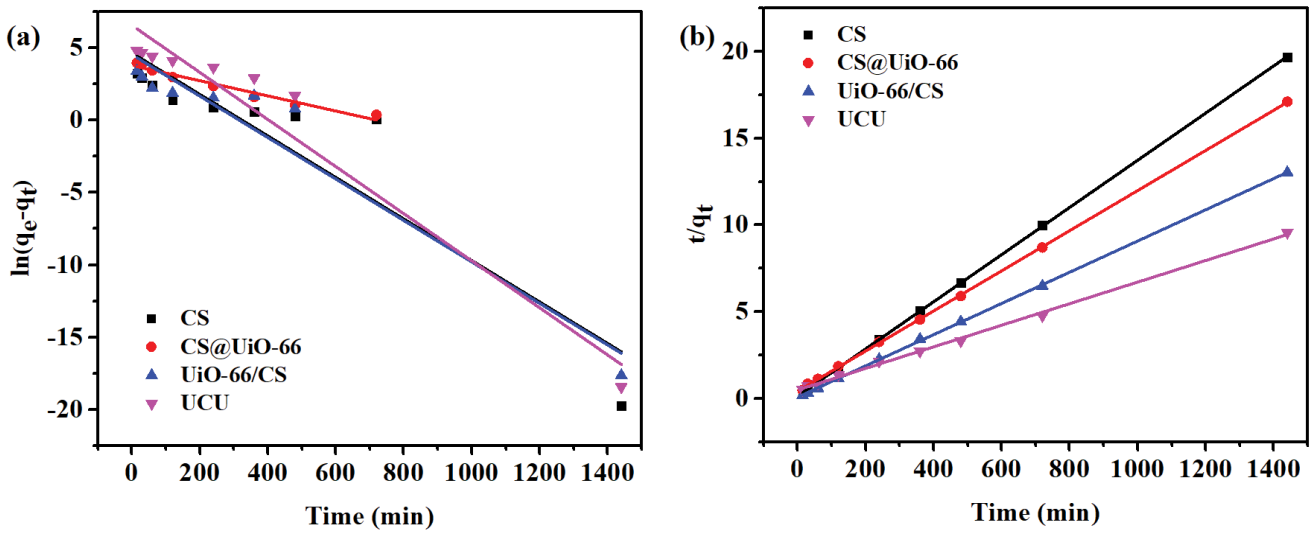

Fig. 8. Kinetic models for adsorption of 2,4-D by four adsorbents. (a) pseudo-first-order kinetic and (b) pseudo-second-order kinetic.

Table 4
Pseudo-first-order and pseudo-second-order kinetic model parameters of adsorption process

Adsorbent	Pseudo-first-order kinetic			Pseudo-second-order kinetic		
	k_1 min^{-1}	q_e mg g^{-1}	R^2	$k_2 \times 10^{-3}$ g mg^{-1} min^{-1}	q_e mg g^{-1}	R^2
CS	0.01436	105.75	0.8278	1.3032	73.58	0.9999
CS@UiO-66	0.00552	44.26	0.9566	0.316	86.51	0.9998
UiO-66/CS	0.01434	93.97	0.9233	0.9612	111.11	0.9998
UCU	0.01628	713.41	0.939	0.078	160.77	0.9978

According to the analysis of the R^2 data's shown in Table 4, it reveals that the adsorption of 2,4-D by four adsorbents can be more suitably described by the pseudo-second-order kinetic model (R^2 > 0.99). The equilibrium adsorption value calculated by the pseudo-second-order kinetic follows the size relationship of UCU > UiO-66/CS > CS@UiO-66 > CS, indicating that UCU has the highest adsorption capacity.

3.3. Adsorption mechanism

3.3.1. Temperature and adsorption thermodynamics

Fig. 9a indicates the effect of temperature on the adsorption of 2,4-D by UCU. As the temperature increases, the adsorption capacity decreases. According to the research on the adsorption in combination with the thermodynamic, we can calculate the three thermodynamic parameters—ΔG (free energy change), ΔH (enthalpy change) and ΔS (entropy change) from the data of Fig. 9. Eqs. (7) and (8) are expressed as follows:

$$\Delta G = -RT \ln K_d \tag{7}$$

$$\ln K_d = \frac{\Delta S}{R} - \frac{\Delta H}{RT} \tag{8}$$

where K_d represents the distribution coefficient; R (J mol^{-1} K^{-1}) refers to the gas constant; T (K) refers to the adsorption temperature. ΔG can be calculated directly by the formula; ΔS and ΔH can be calculated by the intercept and slope of the line in the Van't Hoff plot (Fig. 9b). The calculation results are shown in Table 5. The ΔG stands for a parameter that determines the spontaneousness of the process; the negative value indicates that the adsorption process is spontaneous. The calculated negative ΔH value again proves that the adsorption process is exothermic, which may be caused by the relatively strong electrostatic interaction between the 2,4-D anion and the positively charged adsorbent. ΔS value stands for a parameter describing the degree of chaos in the whole system, and the calculated positive value indicates that the adsorption randomness increases as the temperature rises.

3.3.2. Electrostatic action and pH effect

As an acidic contaminant, the pKa value of 2,4-D is about 2.64. When the pH is lower than the pKa value, the 2,4-D molecule is neutral in the solution, which is not conducive to the exertion of electrostatic action. When the pH rises above the pKa value, the contaminants mainly appear in an anionic form. Fig. 10b shows the ZP curve for UCU. The isoelectric point is observed to be about pH 5.8, and the surface of the adsorbent is positively charged only when the pH is less

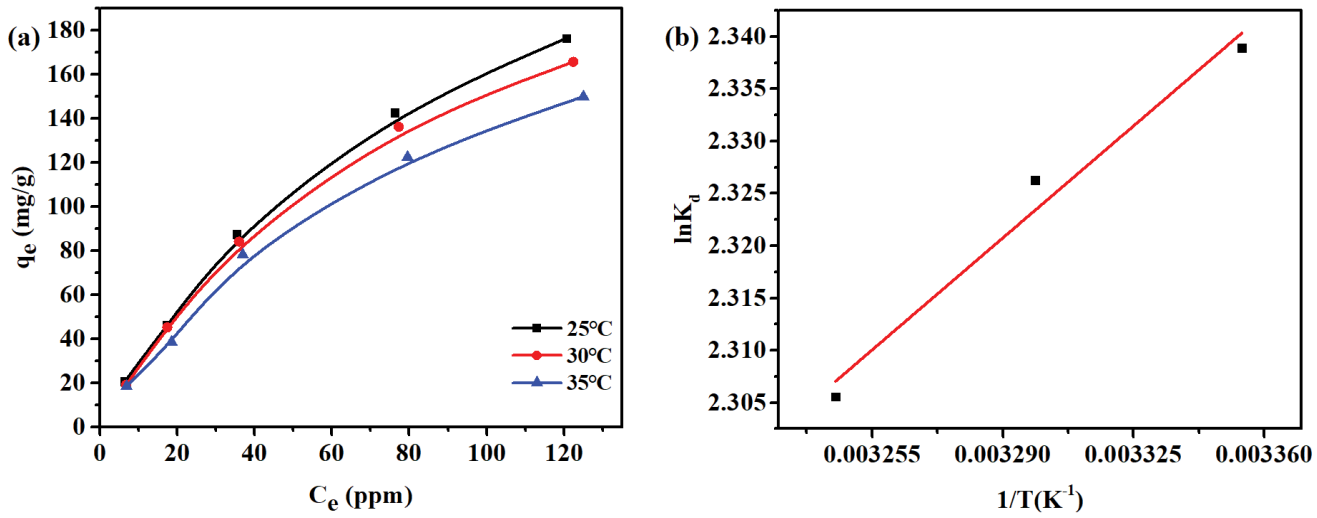

Fig. 9. (a) Adsorption of 2,4-D at different temperatures with UCU and (b) Van't Hoff plot.

Table 5
Thermodynamic parameters for adsorption of 2,4-D by UCU

Temperature K	Adsorption capacity mg g^{-1}	ΔG kJ mol^{-1}	ΔH kJ mol^{-1}	ΔS J mol^{-1} K^{-1}
298	319.49	–5.798	–	–
303	302.11	–5.863	–2.542	10.929
308	272.48	–5.907	–	–

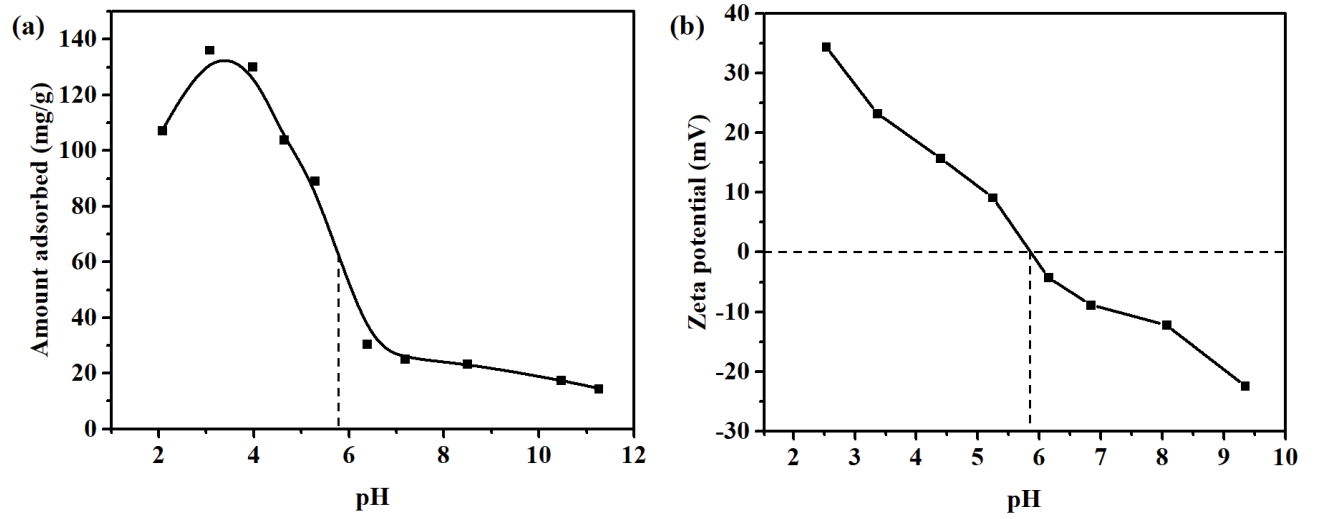

Fig. 10. (a) Effect of pH on adsorption of 2,4-D by UCU and (b) Zeta potential of UCU at different pH.

than 5.8. As shown in Fig. 10a, when the pH is less than 2.64, the neutral 2,4-D molecules in the solution cannot produce positive electrostatic interaction with the adsorbent, resulting in a slight decrease in the adsorption compared to the maximum. When the pH rises from 2.64 to 5.8, the decrease in the amount of adsorption is understandable, considering that the positive charges on the surface of the adsorbent are getting smaller and smaller (during the increase of pH from 3.97 to 5.28, the q_e value decreases from 130.32 to 89.12 mg g^{-1}, which is reduced by about 30%). When the pH is higher than 5.8, the negative charge on the surface of the adsorbent and the 2,4-D anion repel each other, and the electrostatic action is no longer favorable for adsorption (during the increase of pH from 5.28 to 6.38, the q_e value rapidly decreases from 89.12

to 30.59 mg g^{-1}, which is reduced by about 65%). It is foreseen that the adsorption amount is always at a very low level (22.61 mg g^{-1} ±20%). The weak adsorption may be the result of π–π stacking between the benzene rings in UiO-66 and 2,4-D. In summary, pH has a great influence on adsorption, and the recommended pH is from 2.5 to 4.5. The adsorption mechanism is summarized in Fig. 11.

3.4. Effect of interfering contaminants

In order to study the effect of the presence of interfering substances on adsorption, we chose diuron, bentazon and MCPA as interfering substances. The molecular structures of these three herbicides and 2,4-D are shown in Fig. 12. It is worth noting that MCPA and 2,4-D belong to phenoxy

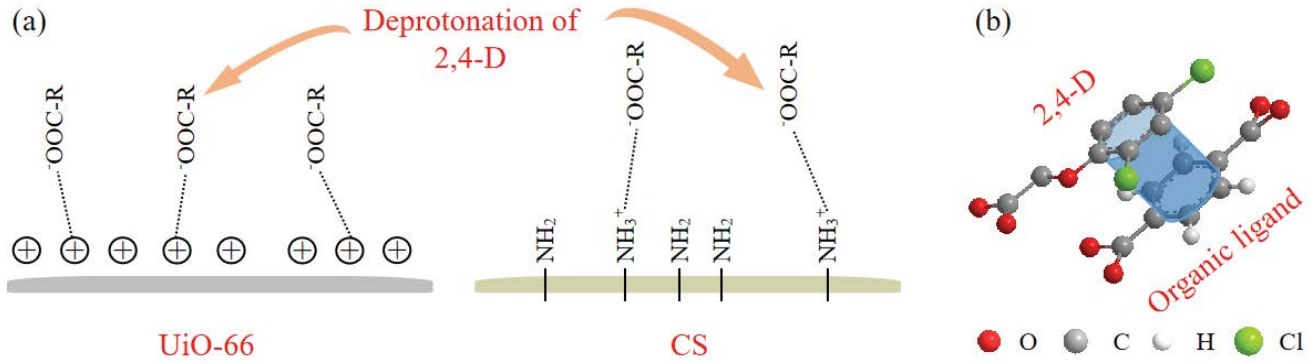

Fig. 11. Adsorption mechanism: (a) Electrostatic interaction of UiO-66 and CS with the deprotonated of 2,4-D and (b) π–π stacking between the benzene rings of UiO-66 ligand and 2,4-D.

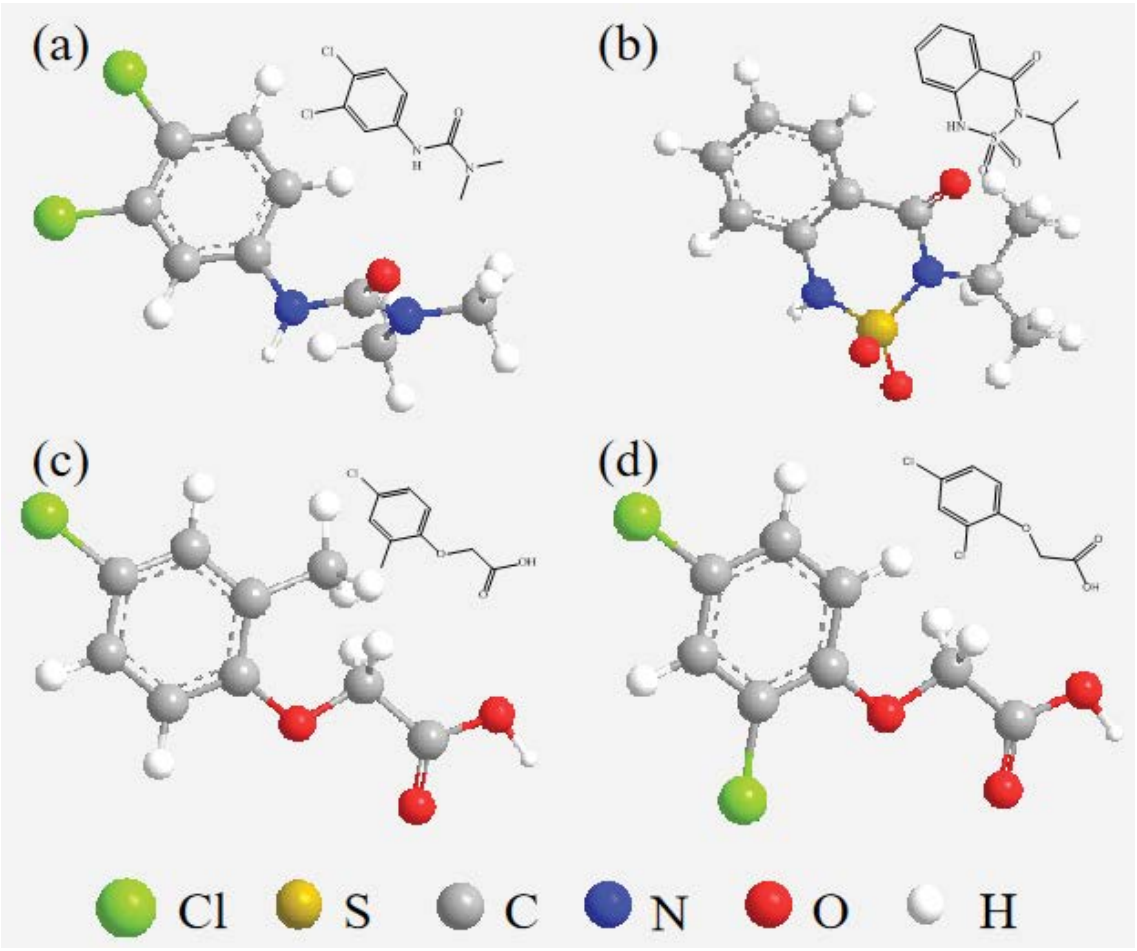

Fig. 12. Molecular structure of the four herbicides, (a) diuron, (b) bentazon, (c) MCPA and (d) 2,4-D.

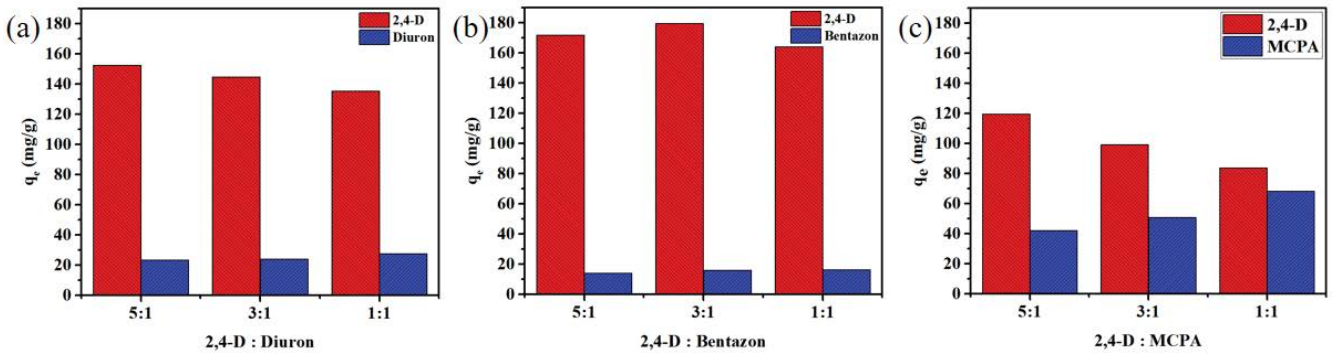

Fig. 13. Effect of different interferents on adsorption: (a) diuron, (b) bentazon and (c) MCPA.

carboxylic acid herbicides, while diuron and bentazone are different species.

According to Lambert-Beer's law, the absorbance of mixed contaminants is measured at a specific wavelength by an ultraviolet spectrophotometer, and the parallel equation is used to obtain the content of a single component in the mixed contaminant. The corresponding wavelength of diuron is 248 nm, bentazon 232 nm and MCPA 279 nm. The expressions of the simultaneous equations are as follows:

$$A_1 = K_1^a bc^a + K_1^b bc^b \quad (9)$$

$$A_2 = K_2^a bc^a + K_2^b bc^b \quad (10)$$

where A_1 and A_2 are the absorbance of the mixed solution measured at two wavelengths, c^a and c^b represent the concentrations of the two single components; K_1^a, K_2^a, K_1^b and K_2^b are the molar absorption coefficients, and b is the optical path.

As shown in Fig. 13, the presence of diuron or bentazon has little interference with the adsorption of 2,4-D, while the effect on the adsorption increases as the concentration of MCPA increases. This indicates that UCU has a similar adsorption capacity for phenoxy carboxylic acid herbicides and is more selective for this type of herbicide. It can be easily inferred that the adsorption of MCPA by UCU uses the same mechanism as adsorption of 2,4-D.

3.5. Recovery and reusability

Reusability is one of the important indicators for the practical application of adsorbents. Considering that 2,4-D can be easily dissolved in ethanol, the adsorbent is desorbed by a mixed solution of ethanol and deionized water (ethanol: water = 3:7). The adsorbed adsorbents were taken out from the 2,4-D solution with tweezers, added to the above mixed solution, and shaken at 150 rpm for 12 h. After being taken out again by tweezers and lyophilized, they were applied in the next cycle. In the first two cycles, almost all CS and UiO-66/CS beads were broken, which could no longer be applied. Although their adsorption capacity is reduced by less than 3% in these two cycles, it is meaningless to measure only their two cycles. As shown in Fig. 14, the adsorption capacity of CS@UiO-66 and UCU can still reach more than 85% when the number of cycles is less than five times. Moreover, when

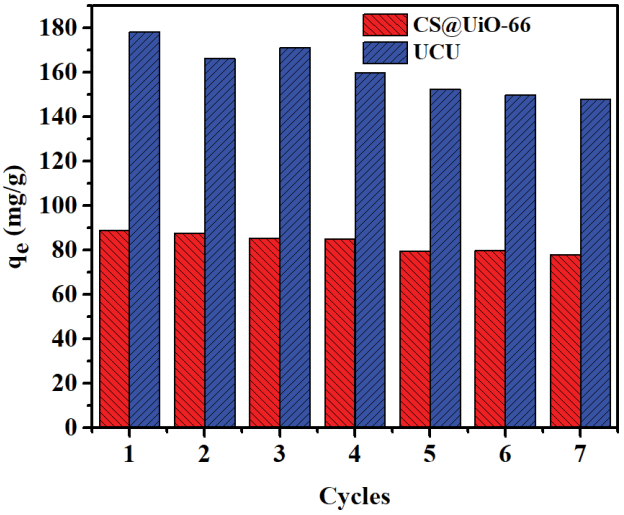

Fig. 14. Reusability of CS@UiO-66 and UCU for the adsorption of 2,4-D.

they cycles seven times, they still maintain a complete bead structure, which is beneficial for practical applications.

3.6. Crushing resistance

During the adsorption process, CS and UiO-66 beads were very fragile, while CS@UiO-66 and UCU was quite different. In this regard, we put the beads into the water to oscillate, controlled speed of the oscillation, and recorded the time for the beads to be broken. Beads (5 mg) were added to water (25 ml) and tested the strength of the beads, by adjusting the oscillatory velocity and calculation time. When the oscillatory velocity was 200 rpm, the CS and UiO-66/CS beads almost all burst at 2 h. At 150 rpm and 180 rpm, these two beads were able to adhere for 20 and 8 h, respectively. Relatively speaking, for CS@UiO-66 and UCU beads, they remained intact after shaking at 200 rpm for 24 h or longer. Fig. 15 shows the variation of four beads over time at 200 rpm. The fragility of CS and UiO-66/CS beads are easy to understand. During the preparation process, lyophilize causes the beads to lose a large amount of moisture, bringing the pores, but at the same time reducing the hardness of the beads. Therefore the CS

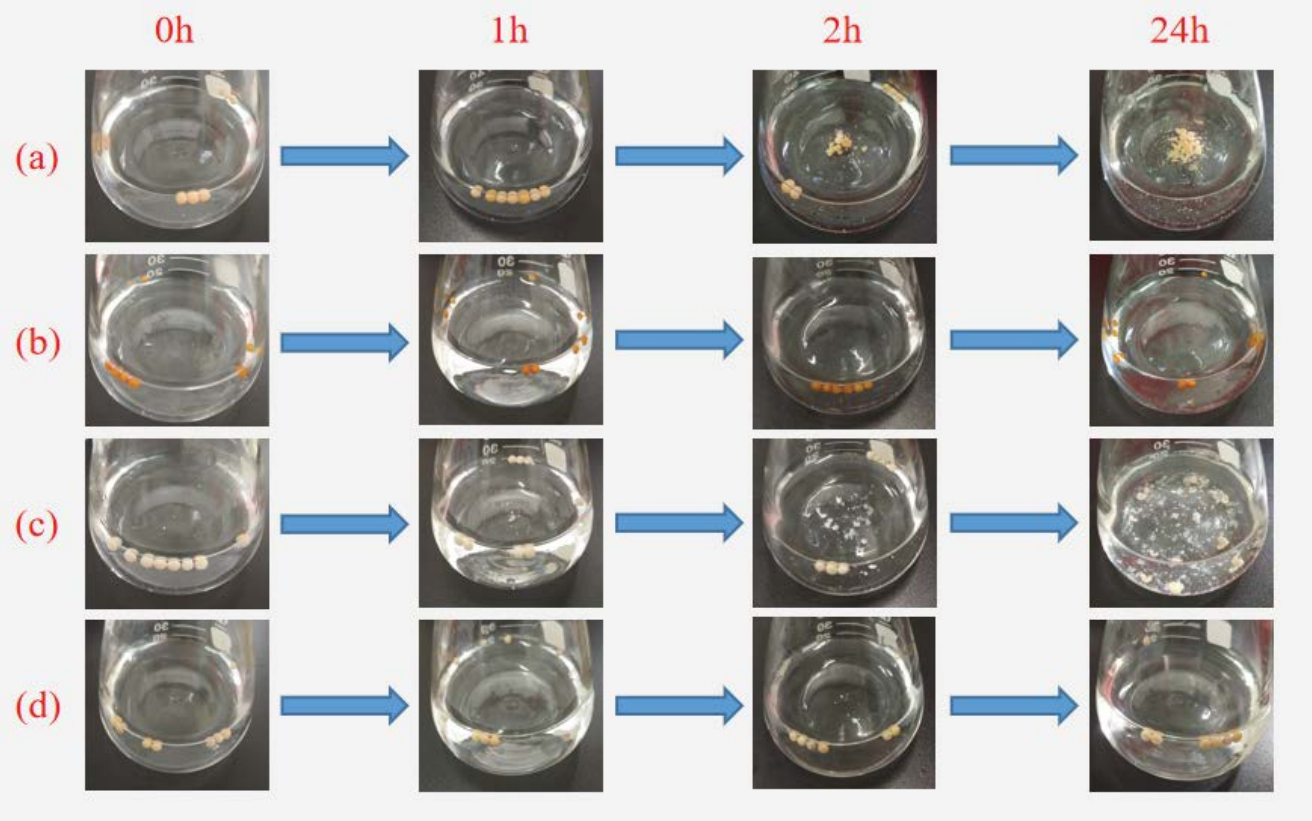

Fig. 15. Preservation of four beads at 200 r min^{-1}: (a) CS bead, (b) CS@UiO-66 bead, (c) UiO-66/CS bead and (d) UCU bead.

beads and the UiO-66/CS beads are fragile. However, CS@UiO-66 and UCU formed a shell composed of CS and UiO-66 due to the surface deposition of UiO-66, which has good resistance to crushing under the protection of the shell.

4. Conclusions

In this research, we successfully fabricated UCU composite bead, which is a novel adsorbent with high adsorption properties. The surface deposition of UiO-66 increases the specific surface area and then enhances crush resistance of the composite bead. The maximum adsorption capacity of UCU for 2,4-D reached 302.1 mg g^{-1}, even higher than many micron or nano materials. Moreover, its capacity decreases little after multiple cycles. Among all the factors for research, the electrostatic effect has the greatest effect on adsorption, and the recommended optimal pH is from 2.5 to 4.5. The adsorption process is dominated by electrostatic interactions, accompanied by the weak influence of π–π stacking. In this way, the excellent adsorption capacity can enhance the crush resistance. Moreover, the superior reusability of UCU millimeter-grade bead can increase the possibility of practical application.

Acknowledgements

The authors sincerely acknowledged the financial supports from the National Natural Science Foundation of China (No. 41371446, No. 41271498 and No. 51204026).

References

[1] T.C. Schmidt, J. Field, Water analysis for emerging chemical contaminants, Anal. Chem., 88 (2016) 1495.
[2] B. Petrie, R. Barden, B. Kasprzyk-Hordern, A review on emerging contaminants in wastewaters and the environment: current knowledge, understudied areas and recommendations for future monitoring, Water Res., 72 (2015) 3–27.
[3] D.N. Bulloch, E.D. Nelson, S.A. Carr, C.R. Wissman, J.L. Armstrong, D. Schlenk, C.K. Larive, Occurrence of halogenated transformation products of selected pharmaceuticals and personal care products in secondary and tertiary treated wastewaters from southern California, Environ. Sci. Technol., 49 (2015) 2044–2051.
[4] Y. Chen, J. Vymazal, T. Březinova, M. Koželuh, L. Kule, J.G. Huang, Z.B. Chen, Occurrence, removal and environmental risk assessment of pharmaceuticals and personal care products in rural wastewater treatment wetlands, Sci. Total Environ., 566–567 (2016) 1660–1669.
[5] S.D. Richardson, T.A. Ternes, Water analysis: emerging contaminants and current issues, Anal. Chem., 86 (2014) 2813–2848.
[6] S.D. Richardson, S.Y. Kimura, Water analysis: emerging contaminants and current issues, Anal. Chem., 88 (2016) 546–582.
[7] A.L. Spongberg, J.D. Witter, J. Acuña, J. Vargas, M. Murillo, G. Umaña, E. Gómez, G. Perez, Reconnaissance of selected PPCP compounds in Costa Rican surface waters, Water Res., 45 (2011) 6709–6717.
[8] Q. Sun, M. Li, C. Ma, X. Chen, X. Xie, C.P. Yu, Seasonal and spatial variations of PPCP occurrence, removal and mass loading in three wastewater treatment plants located in different urbanization areas in Xiamen, China, Environ. Pollut., 208 (2016) 371–381.

[9] L.K. Dodgen, J. Li, D. Parker, J.J. Gan, Uptake and accumulation of four PPCP/EDCs in two leafy vegetables, Environ. Pollut., 182 (2013) 150–156.
[10] T. Eggen, C. Lillo, Antidiabetic II drug metformin in plants: uptake and translocation to edible parts of cereals, oily seeds, beans, tomato, squash, carrots, and potatoes, J. Agric. Food. Chem., 60 (2012) 6929–6935.
[11] A.K. Hotchkiss, C.V. Rider, C.R. Blystone, V.S. Wilson, P.C. Hartig, G.T. Ankley, P.M. Foster, C.L. Gray, L.E. Gray, Fifteen years after "Wingspread" – environmental endocrine disrupters and human and wildlife health: where we are today and where we need to go, Toxicol. Sci., 105 (2008) 235–259.
[12] B. Kurenbach, D. Marjoshi, C.F. Ambile-Cuevas, G.C. Ferguson, W. Godsoe, P. Gibson, J.A. Sublethal exposure to commercial formulations of the herbicides dicamba, 2,4-dichlorophenoxyacetic acid, and glyphosate cause changes in antibiotic susceptibility in *Escherichia coli* and *Salmonella enterica serovar Typhimurium*, Heinemann, Mbio., 6 (2015) pii: e00009–15.
[13] A.M. Browne, P.A. Moore, The effects of sublethal levels of 2,4-dichlorophenoxyacetic acid herbicide (2,4-D) on feeding behaviors of the crayfish *O. rusticus*, Arch. Environ. Contam. Toxicol., 67 (2014) 234–244.
[14] M.B. Gilliard, C.A. Martín, A.E. Cassano, M.E. Lovato, Reaction kinetic model for 2,4-dichlorophenoxyacetic acid decomposition in aqueous media including direct photolysis, direct ozonation, ultraviolet C, and pH enhancement, Ind. Eng. Chem. Res., 52 (2013) 14034–14048.
[15] M. Kuster, M.J.L. de Alda, M.D. Hernando, M. Petrovic, J. Martín-Alonso, D. Barceló, Analysis and occurrence of pharmaceuticals, estrogens, progestogens and polar pesticides in sewage treatment plant effluents, river water and drinking water in the Llobregat river basin (Barcelona, Spain), J. Hydrol., 358 (2008) 112–123.
[16] R. Loos, G. Locoro, S. Comero, S. Contini, D. Schwesig, F. Werres, P. Balsaa, O. Gans, S. Weiss, L. Blaha, M. Bolchi, B.M. Gawlik, Pan-European survey on the occurrence of selected polar organic persistent pollutants in ground water, Water Res., 44 (2010) 4115–4126.
[17] L. Tang, S. Zhang, G.-M. Zeng, Y. Zhang, G.-D. Yang, J. Chen, J.-J. Wang, J.-J. Wang, Y.-Y. Zhou, Y.-C. Deng, Rapid adsorption of 2,4-dichlorophenoxyacetic acid by iron oxide nanoparticles-doped carboxylic ordered mesoporous carbon, J. Colloid Interface Sci., 445 (2015) 1–8.
[18] M.A. Peterson, S.A. McMaster, D.E. Riechers, J. Skelton, P.W. Stahlman, 2,4-D past, present, and future: a review, Weed Technol., 30 (2016) 303–345.
[19] L. Yang, W. Sun, S.L. Luo, Y. Luo, White fungus-like mesoporous Bi_2S_3 ball/TiO_2 heterojunction with high photocatalytic efficiency in purifying 2,4-dichlorophenoxyacetic acid/Cr(VI) contaminated water, Appl. Catal., B, 156–157 (2014) 25–34.
[20] S. Sandeep, K.L. Nagashree, T. Maiyalagan, G. Keerthiga, Photocatalytic degradation of 2,4-dichlorophenoxyacetic acid - a comparative study in hydrothermal TiO_2 and commercial TiO_2, Appl. Surf. Sci., 156–157 (2014) 25–34.
[21] J.-y. Ma, X.-c. Quan, Z.-f. Yang, A.-j. Li, Biodegradation of a mixture of 2,4-dichlorophenoxyacetic acid and multiple chlorophenols by aerobic granules cultivated through plasmid pJP4 mediated bioaugmentation, Chem. Eng. J., 181–182 (2012) 144–151.
[22] B. Carboneras, J. Villaseñor, F.J. Fernandez-Morales, Modelling aerobic biodegradation of atrazine and 2,4-dichlorophenoxy acetic acid by mixed-cultures, Bioresour. Technol., 243 (2017) 1044–1050.
[23] N. Jaafarzadeh, F. Ghanbari, M. Ahmadi, Efficient degradation of 2,4-dichlorophenoxyacetic acid by peroxymonosulfate/magnetic copper ferrite nanoparticles/ozone: a novel combination of advanced oxidation processes, Chem. Eng. J., 320 (2017) 436–447.
[24] D. Angin, A. Ilci, Removal of 2,4-dichlorophenoxy acetic acid from aqueous solutions by using activated carbon derived from olive-waste cake, Desal. Wat. Treat., 82 (2017) 282–291.
[25] S.M. Pourmortazavi, M. Taghdiri, R. Ahmadi, M.M. Zahedi, Procedure optimization for removal of 2,4-dichlorophenoxyacetic acid from water by surfactant-modified magnetic nanoparticles, Desal. Wat. Treat., 70 (2017) 261–268.
[26] Z. Hasan, E.-J. Choi, S.H. Jhung, Adsorption of naproxen and clofibric acid over a metal–organic framework MIL-101 functionalized with acidic and basic groups, Chem. Eng. J., 219 (2013) 537–544.
[27] B.K. Jung, Z. Hasan, S.H. Jhung, Adsorptive removal of 2,4-dichlorophenoxyacetic acid (2,4-D) from water with a metal–organic framework, Chem. Eng. J., 234 (2013) 99–105.
[28] D.-M. Chen, X.-H. Liu, N.-N. Zhang, C.-S. Liu, M. Du, Immobilization of polyoxometalate in a cage-based metal–organic framework towards enhanced stability and highly effective dye degradation, Polyhedron, 152 (2018) 108–113.
[29] X.L. Liu, N.K. Demir, Z.T. Wu, K. Li, Highly water-stable zirconium metal–organic framework UiO-66 membranes supported on alumina hollow fibers for desalination, J. Am. Chem. Soc., 137 (2015) 6999–7002.
[30] N. Zhuo, Y.Q. Lan, W.B. Yang, Z. Yang, X.M. Li, X. Zhou, Y. Liu, J.C. Shen, X.T. Zhang, Adsorption of three selected pharmaceuticals and personal care products (PPCPs) onto MIL-101(Cr)/natural polymer composite beads, Sep. Purif. Technol., 177 (2017) 272–280.
[31] L.L. Zhai, Z.S. Bai, Y. Zhu, B.J. Wang, W.Q. Luo, Fabrication of chitosan microspheres for efficient adsorption of methyl orange, Chin. J. Chem. Eng., 26 (2018) 657–666.
[32] L. Maddalena, F. Carosio, J. Gomez, G. Saracco, A. Fina, Layer-by-layer assembly of efficient flame retardant coatings based on high aspect ratio graphene oxide and chitosan capable of preventing ignition of PU foam, Polym. Degrad. Stab., 152 (2018) 1–9.
[33] J.J. Wu, T. Zhou, J.Y. Liu, Y. Wan, Injectable chitosan/dextran-polylactide/glycerophosphate hydrogels and their biodegradation, Polym. Degrad. Stab., 120 (2015) 273–282.
[34] Z. Al-Qodah, M.A. Yahya, M. Al-Shannag, On the performance of bioadsorption processes for heavy metal ions removal by low-cost agricultural and natural by-products bioadsorbent: a review, Desal. Wat. Treat., 85 (2017) 339–357.
[35] Y.S. Açıkel, B. Göze, Removal of Methyl Red, a cationic dye, Acid Blue 113, an anionic dye, from wastewaters using chitin and chitosan: influence of copper ions, Desal. Wat. Treat., 73 (2017) 289–300.
[36] R. Ahmad, I. Hasan, A. Mittal, Adsorption of Cr (VI) and Cd (II) on chitosan grafted polyaniline-OMMT nanocomposite: isotherms, kinetics and thermodynamics studies, Desal. Wat. Treat., 58 (2017) 144–153.
[37] P. Hu, L.J. Zhang, J. Wang, R.H. Huang, Removal of methyl orange from aqueous solution with crosslinked quaternized chitosan/bentonite composite, Desal. Wat. Treat., 80 (2017) 370–379.
[38] P. Hu, J. Wang, R.H. Huang, Adsorption of Cr(VI) and methyl orange from aqueous solutions by quaternized chitosan immobilized bentonite, Desal. Wat. Treat., 65 (2017) 435–442.
[39] G. Dilarri, R.N. Montagnolli, E.D. Bidoia, C.R. Mendes, C.R. Corso, Kinetic, isothermal, and thermodynamic models to evaluate Acid Blue 161 dye removal using industrial chitosan powder, Desal. Wat. Treat., 109 (2018) 261–270.
[40] T. Zhou, L.Y. Fang, X.W. Wang, M.Y. Han, S.S. Zhang, R.P. Han, Adsorption of the herbicide 2,4-dichlorophenoxyacetic acid by Fe-crosslinked chitosan complex in batch mode, Desal. Wat. Treat., 70 (2017) 294–301.
[41] Z. Hasan, N.A. Khan, S.H. Jhung, Adsorptive removal of diclofenac sodium from water with Zr-based metal–organic frameworks, Chem. Eng. J., 284 (2016) 1406–1413.
[42] Q.S. Fu, L. Wen, L. Zhang, X.D. Chen, D. Pun, A. Ahmed, Y.H. Yang, H.F. Zhang, Preparation of Ice-templated MOF–polymer composite monoliths and their application for wastewater treatment with high capacity and easy recycling, ACS Appl. Mater. Interfaces, 9 (2017) 33979–33988.
[43] L. Valenzano, B. Civalleri, S. Chavan, S. Bordiga, M.H. Nilsen, S. Jakobsen, K.P. Lillerud, C. Lamberti, Disclosing the complex structure of UiO-66 metal organic framework: a synergic combination of experiment and theory, Chem. Mater., 23 (2011) 1700–1718.

[44] S. Chavan, J.G. Vitillo, D. Gianolio, O. Zavorotynska, B. Civalleri, S. Jakobsen, M.H. Nilsen, L. Valenzano, C. Lamberti, K.P. Lillerud, S. Bordiga, H_2 storage in isostructural UiO-67 and UiO-66 MOFs, Phys. Chem. Chem. Phys., 14 (2012) 1614–1626.
[45] K. Kuśmierek, M. Szala, A. Świątkowski, Adsorption of 2,4-dichlorophenol and 2,4-dichlorophenoxyacetic acid from aqueous solutions on carbonaceous materials obtained by combustion synthesis, J. Taiwan Inst. Chem. Eng., 63 (2016) 371–378.
[46] S. Manna, P. Saha, D. Roy, R. Sen, B. Adhikari, Removal of 2,4-dichlorophenoxyacetic acid from aqueous medium using modified jute, J. Taiwan Inst. Chem. Eng., 67 (2016) 292–299.
[47] V.O. Njoku, Md. A. Islam, M. Asif, B.H. Hameed, Adsorption of 2,4-dichlorophenoxyacetic acid by mesoporous activated carbon prepared from H_3PO_4-activated langsat empty fruit bunch, J. Environ. Manage., 154 (2015) 138–144.
[48] S. Nethaji, A. Sivasamy, Graphene oxide coated with porous iron oxide ribbons for 2, 4-Dichlorophenoxyacetic acid (2,4-D) removal, Ecotoxicol. Environ. Saf., 138 (2017) 292–297.
[49] S. Zhong, C.Y. Zhou, X.N. Zhang, H. Zhou, H. Li, X.H. Zhu, Y. Wang, A novel molecularly imprinted material based on magnetic halloysite nanotubes for rapid enrichment of 2,4-dichlorophenoxyacetic acid in water, J. Hazard. Mater., 276 (2014) 58–65.
[50] O. Kazak, Y.R. Eker, I. Akin, H. Bingol, A. Tor, Green preparation of a novel red mud@carbon composite and its application for adsorption of 2,4-dichlorophenoxyacetic acid from aqueous solution, Environ. Sci. Pollut. Res., 24 (2017) 23057–23068.